A simplified approach to determine aerodynamic damping of railway overheads

S. Avila-Sanchez [a], O. Lopez-Garcia [b], J. Meseguer [c]

IDR/UPM,Universidad Politécnica de Madrid, Madrid, Spain
[a] s.avila@upm.es, [b] oscar.lopez.garcia@upm.es, [c] j.meseguer@upm.es

1 INTRODUCTION

The railway overhead (or catenary) is the system of cables responsible for providing electric current to the train. This system has been reported as wind-sensitive (Scanlon et al., 2000), and particularly to the occurrence of galloping phenomena. Galloping phenomena of the railway overhead consists of undamped cable oscillations triggered by aerodynamic forces acting on the contact wire. As is well known, aerodynamic loads on the contact wire depends on the incident flow mean velocity and the angle of attack. The presence of embankments or hills modifies both vertical velocities profiles and angles of attack of the flow (Paiva et al., 2009). The presence of these cross-wind related oscillations can interfere with the safe operation of the railway service (Johnson, 1996). Therefore a correct modelling of the phenomena is required to avoid these unwanted oscillations.

The railway overhead is composed of three different cables, messenger, droppers and contact wires (Fig. 1*a*). The catenary stiffness depends on the distance to the centre of the span, see for instance Lopez-Garcia et al. (2007). However, it can be approximated to a spring with periodic stiffness distribution in order to establish a one degree of freedom (ODOF) equivalent system (Wu and Brennan, 1998) to study the dynamic interaction between catenary and pantograph. This approach simplifies the determination of the contact lose between both elements, but complicates the characterization of the aerodynamic damping on the equivalent system. In the simple approach herein presented, the stiffness distribution is assumed constant, i.e., a catenary span is represented as a one-dimensional oscillator, as shown in Figure 1.

Aerodynamic loads caused by an incident flow can lead to the appearance of undamped displacements (Stickland and Scanlon, 2001). The motion of the one-dimensional ODOF system, $y(t)$, exposed to an incident flow (Fig. 1*b*) is determined by the following differential equation

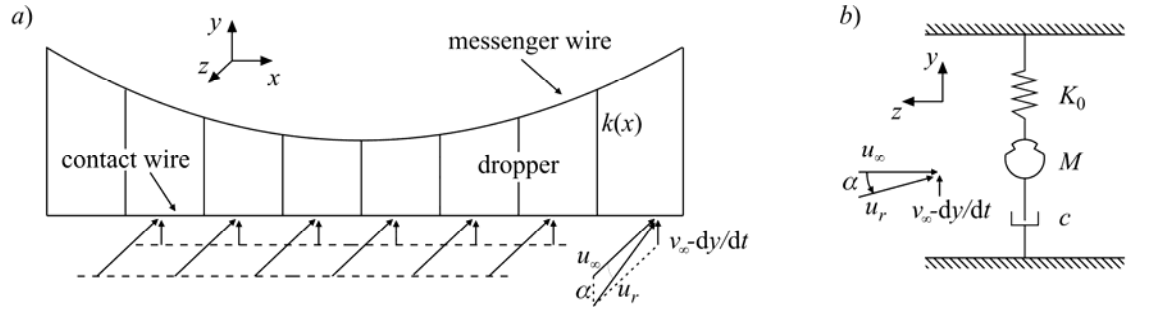

Figure 1. Simplification of a catenary span (*a*) to a one degree of freedom oscillator (*b*) exposed to a steady incident wind flow.

$$\frac{\mathrm{d}^2 y(t)}{\mathrm{d}t^2}+\frac{c_s}{M}\frac{\mathrm{d}y(t)}{\mathrm{d}t}+\frac{K_0}{M}y(t)=\frac{\rho S}{2M}u_r^2\left(c_l(\alpha)\cos\alpha+c_d(\alpha)\sin\alpha\right) \tag{1}$$

where c_s stands for the structural damping coefficient, M for the equivalent mass, K_0 for the average stiffness of the catenary, ρ is the air density, S stands for the reference area, u_r is the relative wind speed, c_l the lift coefficient of the contact wire, c_d the drag coefficient, and α the angle of attack. The angle of attack is defined as $\alpha = \text{atan}\,(v_\infty - \mathrm{d}y/\mathrm{d}t)/u_\infty$, where u_∞ and v_∞ are the horizontal and vertical velocity of the incident flow, respectively.

Some simplifications can be introduced in Equation 1 in order to study one-dimensional galloping. Assuming $\alpha \sim (v_\infty - \mathrm{d}y/\mathrm{d}t)/u_\infty << 1$, the linearized motion equation is

$$\frac{\mathrm{d}^2 y(t)}{\mathrm{d}t^2}+2(\zeta_s+\zeta_a)\omega_n\frac{\mathrm{d}y(t)}{\mathrm{d}t}+\omega_n^2 y(t)=2\zeta_a\omega_n v_\infty \tag{2}$$

where ζ_s is the structural damping ratio, defined as $\zeta_s = c_s/(2M\omega_n)$, ζ_a is the aerodynamic damping ratio and ω_n is the natural frequency. Note that the aerodynamic damping ratio is

$$\zeta_a=\frac{\rho S u_\infty}{4M\omega_n}H(\alpha) \tag{3}$$

where $H(\alpha)$ stands for den-Hartog coefficient (Alonso et al., 2007), $H(\alpha) = c_{l\alpha}(\alpha)+c_d(\alpha)$, and $c_{l\alpha}$ is the lift coefficient slope. The structural damping ratio is always positive, but the aerodynamic damping ratio can be negative if $H(\alpha)$ is negative. Therefore, the one-dimensional ODOF system can gallop only if $H(\alpha) < 0$ and the incident wind speed is larger than the galloping speed , $u_d = -4M\omega_n\zeta_s/(\rho S H(\alpha))$, (Stickland and Scanlon, 2001).

The logarithmic decrement, δ, of the displacement $y(t)$ is the natural logarithm of the amplitude, Y, of two peaks separated n periods, i.e., $\delta = \ln(Y_0/Y_n)/n$. As is well-known, the logarithmic decrement is related to the structural and aerodynamic damping ratios, as

$$\delta=\frac{2\pi(\zeta_s+\zeta_a)}{\sqrt{1-(\zeta_s+\zeta_a)^2}} \tag{4}$$

As can be appreciated, both the structural and aerodynamic damping ratios are related in the general problem. For the sake of simplicity, the structural damping ratio is neglected in order to characterise the aerodynamic damping ratio. Therefore, in the present analysis the aerodynamic logarithmic decrement, in the absence of structural damping, is defined as

$$\delta_{a0}=\frac{2\pi\zeta_a}{\sqrt{1-\zeta_a^2}} \tag{5}$$

In the present study, experimental aerodynamic coefficients of the contact wire are obtained, and the logarithmic decrement is used to compare aerodynamic damping ratios corresponding to the simplified model (Eq. 2) and the non-linear one-dimensional ODOF system (Eq. 1).

2 EXPERIMENTAL SET-UP

The cross-section of a typical contact wire is a non-circular one that may exhibit galloping phenomena. In order to determine the contact wire aerodynamic load coefficients, wind tunnel tests were carried out. The contact wire analysed corresponds to one of the typical contact wires used in the Spanish railway system, and consists of a cylinder with a nearly circular cross-section with two grooves, as sketched in Figure 2.

The contact between catenary and pantograph causes friction which in the long term evidently wears both elements, modifying the shape of the wire. Wear modifies the aerodynamic properties of the contact wire (Stickland and Scanlon, 2001), but the contact wire is not replaced while the wear effects are lower than a threshold value (maximum admissible wear). In order to take into account the wear effect, three different cross-sections have been studied: contact wire with no wear (Fig. 2*a*), with low wear (Fig. 2*b*), and with maximum admissible wear (Fig. 2*c*). The diameter of the contact wire mock-up with no wear is $d_0 = 64$ mm, being the corresponding aspect ratio $L_0/d_0 \sim 2.3$, where L_0 is the width of the model. The three mock-ups were analysed at a scale 5:1.

An open-circuit wind tunnel with a closed test section has been used to perform the set of two-dimensional tests (Figure 3). The working section is 0.8 m high, 0.15 m wide and 1.2 m long. A 6-components strain gauge load cell, model ATI Gamma SI-130-10, has been used to determine the aerodynamic loads on the contact wire mock-up.

The dynamic pressure, $q = \rho u_r^2/2$, has been obtained with an Air Flow 048 pitot tube, connected to the Schaewitz Lucas P-3061-2WD pressure transducer. The Reynolds number is $\mathrm{Re} = u_r d_0/\nu$, where $\nu \cong 1.5\times10^{-5}$ m^2/s is the kinematic viscosity. The wind speed at the test section was about 10 m/s. The Reynolds number is about 4.3×10^4 in the case of wire with no wear. Because the contact wire cross-section is symmetric, only angles of attack from $\alpha = -90$ to $\alpha = 90$ were analysed. At each angular position, the aerodynamic loads and the dynamic pressure were acquired sampling at 100 Hz during 10 s (these values were chosen as the appropriate values after trying different sampling rates and periods).

As is well-known the lift and aerodynamic drag coefficients are defined as, $c_l = L/(qB_0)$ and $c_d = \mathrm{D}/(qB_0)$, respectively, where L is the lift force, D the aerodynamic drag, q is the dynamic pressure and B_0 is the frontal area of the contact wire mock-up with no wear. The aerodynamic coefficients of the catenary contact wire are computed as the mean values of the acquired aerodynamic coefficient time series.

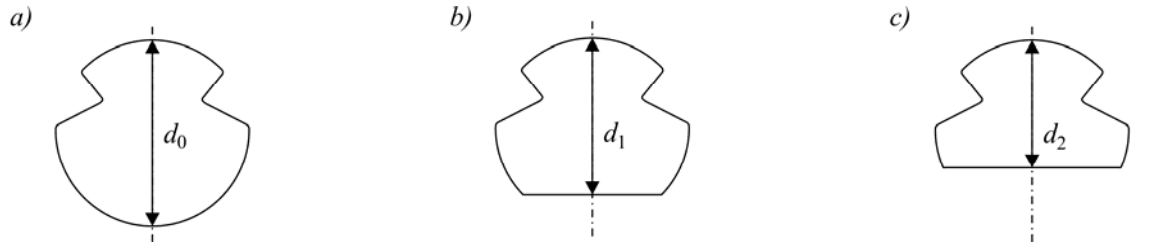

Figure 2. Sketch of the contact wire cross-sections used at the experimental tests. a) wire with no wear ($d_0 = 64$ mm), b) section with low wear ($d_1 = 53$ mm), c) wire with the highest admissible wear ($d_2 = 43$ mm).

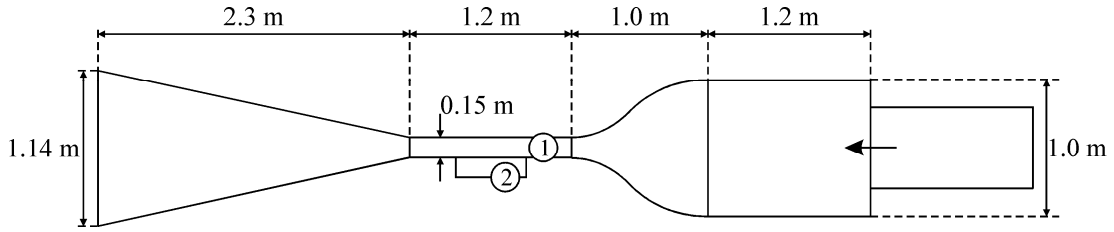

Figure 3. Top view of the wind tunnel used to perform the tests, with some representative dimensions. The tests chamber is located in 1. The strain gauge load cell is located inside the access door to the test chamber 2.

3 EXPERIMENTAL RESULTS

Experimental results corresponding to den-Hartog coefficient, $H(\alpha)$, as function of the angle of attack, α, are shown in Figure 4. For those angles of attack with $H(\alpha) < 0$, galloping phenomena may occur. For low angles of incidence of the flow and the contact wire with no wear effect, the galloping phenomena does not appear based on den-Hartog criteria. If a low wear effect is introduced, a galloping instability may occur for low and positive values of the angle of attack. However, the range of angles of attack in which this instability happens is larger and is displaced towards the negative region, in the model with the highest admissible wear. Also, an increase on the wear effect seems to worsen the effect of the instability for lower angles of attack.

It should be pointed out that there exist differences with results obtained by Stickland and Scanlon (2001). Two reasons may lay behind such apparent differences. First, both tests were performed independently; therefore the wind tunnels used in the tests, the analysed cross-section geometry, and the upstream flow condition are different in both studies. Second, the contact wire geometries used in both studies may differ, and as reported by Stickland and Scanlon slight differences in the cross-section geometry of the contact wire can produce larger qualitative differences in the aerodynamic loads. This effect can also be appreciated in the results herein presented.

The aerodynamic logarithmic decrement, δ_{a0}, defined in Equation 5 for angles of attack from $\alpha = -10º$ to $\alpha = 10º$ is presented in Figure 5. In order to compute the aerodynamic logarithmic decrement, the reference area is chosen as $B_0 = d_0 l$, where $l = 50$ m is the length of one catenary span. The mass of the span is approximated as $M \sim 84$ kg, based on density values reported by Cho (2008). The circular natural frequency is chosen as $\omega_n \sim 1.4$ rad/s (Stickland and Scanlon, 2001).

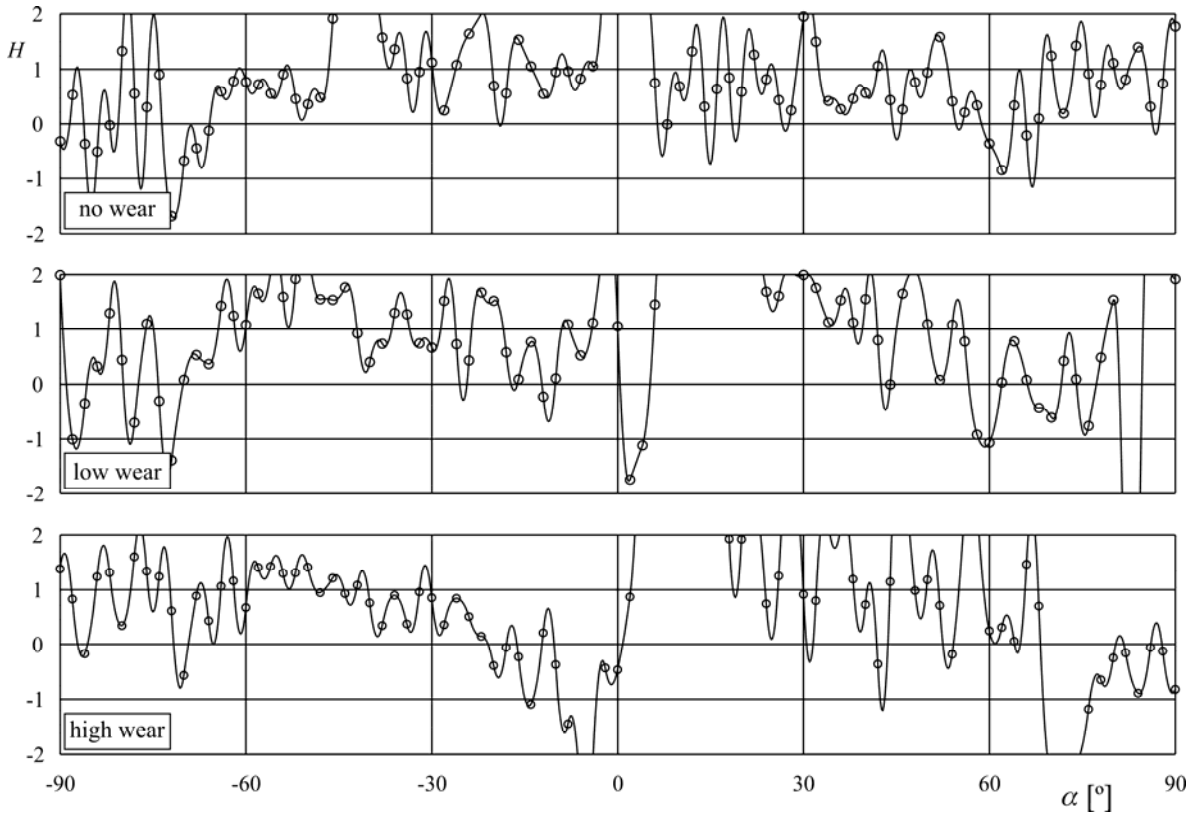

Figure 4. den-Hartog coefficient, H, as function of the angle of attack, α, for the three contact wires analysed.

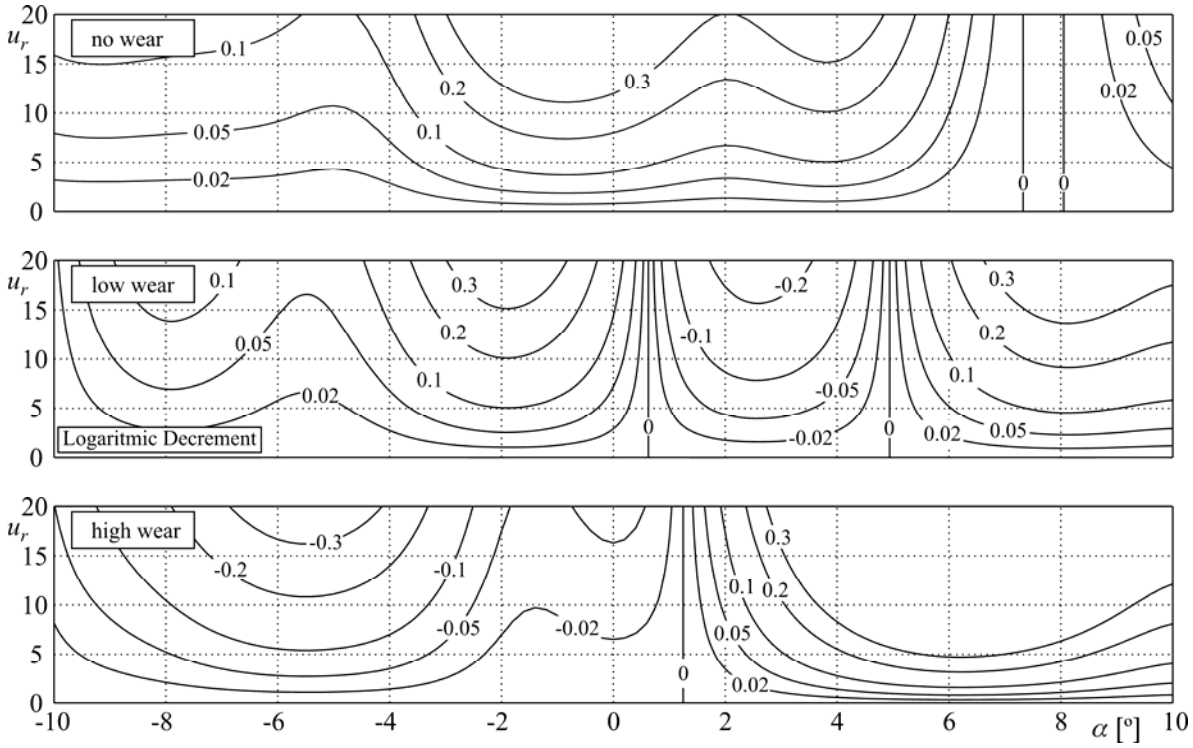

Figure 5. Aerodynamic logarithmic decrement, δ_{a0}, corresponding to the linear model shown in equation 5, as function of the angle of incidence of the flow, α, and the incident flow wind speed, u_r, for the catenary contact wires with low wear.

Results shown in Figure 5 correspond to the aerodynamic logarithmic decrement for the linear model, as shown in Equation 5. Consequently they provide qualitative information quite similar to den-Hartog criteria, but they also provide a more simple perspective of the degree in which the oscillations decay or are amplified, as function of the velocity of the incident flow. Typical structural damping ratios are lower than $\zeta_s < 0.05$ ($\delta_s < 0.31$, approx.) in many cable structures (Macdonald, 2002). As can be seen in the results, this first approximation provides values which are similar to the typical values of the structural damping ratio for those angles of attack with $H(\alpha) > 0$ ($\delta_a > 0$). Therefore, if the aerodynamic damping ratio is positive, and the incident wind speed is high enough, the aerodynamic contribution to the damping coefficient is at least of the same order of magnitude to the structural one.

4 CONCLUSIONS AND DISCUSSION

Most of the studies related to catenary-pantograph interaction simplify the equivalent damping ratio to constant values to elude the characterization of the aerodynamic contribution. In this document a simplified model to estimate the aerodynamic damping ratio, assuming both quasi-static angles of attack and absence of structural damping is used. Despite the limitations of this approach, when the aerodynamic contribution counteracts the apparition of galloping phenomena, the aerodynamic contribution is comparable to the typical structural one. However, the damping ratios provided by this first approach are lower than the damping ratio used by Wu and Brennan (1998). A more thoughtful insight to the model should be undertaken in future to take into consideration the non-linear effects and the three-dimensional nature of the problem.

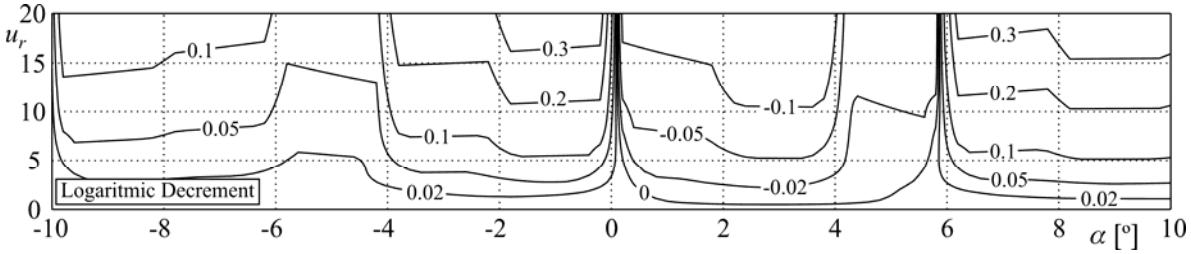

Figure 6. Aerodynamic logarithmic decrement, δ_{a0}, corresponding to the complete non-linear model in equation 1, when the initial condition to compute the oscillation is $\Delta y_0 = 0.2$ m, as function of the angle of incidence of the flow, α, and the incident flow wind speed, u_r, for the catenary contact wire with low wear effect.

As a first attempt to compare the effect of the nonlinearities, Equation 1 can be integrated in order to compute the corresponding aerodynamic logarithmic decrement, as shown in Figure 6 for the contact wire with low wear effect taking as initial condition a displacement $\Delta y_0 = 0.2$ m. As is shown, nonlinearities introduce significant changes in the stability map shown in Figure 5, but they also depend on the initial conditions used. However, this approach has some limitations. Higher order approximations introduce non-linear effects on the aerodynamic damping ratio, modifying its value during the oscillation. Therefore it should be considered the shape of the of the aerodynamic coefficient in the direction of the oscillation (Barrero et al., 2009) and the existence of possible limit cycles.

5 ACKNOWLEDGEMENTS

This work has been supported by the Spanish Ministerio de Ciencia e Innovación, under contract TRA2009-13912-C012-01.

6 REFERENCES

Alonso, G., Meseguer, J., Pérez-Grande, I., 2007. Galloping stability of triangular cross-sectional bodies: A systematic approach. Journal of Wind Engineering and Industrial Aerodynamics 95, 928–940.

Barrero-Gil, A., Sanz-Andrés, A., Alonso, G. 2009. Hysteresis in transverse galloping: The role of the inflection points. Journal of Fluids and Structures 25, 1007–1020

Cho, Y.H., 2008. Numerical simulation of the dynamic responses of railway overhead contact lines to a moving pantograph, considering a nonlinear dropper. Journal of Sound and Vibration 315, 433–454

Johnson, T., 1996. Strong wind effects on railway operations - 16th October 1987. Journal of Wind Engineering and Industrial Aerodynamics 60, 251-266.

Lopez-Garcia, O., Carnicero, A., Maroño, J.L., 2007. Influence of stiffness and contact modelling on catenary–pantograph system dynamics. Journal of Sound and Vibration 299, 806–821.

Macdonald, J.H.G., 2002. Separation of the contributions of aerodynamic and structural damping in vibrations of inclined cables. Journal of Wind Engineering and Industrial Aerodynamics 90, 19–39

Paiva, L.M.S., Bodstein, G.C.R., Menezes, W.F., 2009. Numerical simulation of atmospheric boundary layer flow over isolated and vegetated hills using RAMS. Journal of Wind Engineering and Industrial Aerodynamics 97, 439-454.

Scanlon, T. J., Stickland, M., Oldroyd, A., 2000. An investigation into the attenuation of wind speed by the use of windbreaks in the vicinity of overhead wires. Proc. Instn. Mech. Engrs, Part F. J. Rail and Rapid Transit 214, 173–182.

Stickland, M., Scanlon, T. J., 2001. An investigation into the aerodynamic characteristics of catenary contact wires in a cross-wind. Proc. Instn. Mech. Engrs, Part F. J. Rail and Rapid Transit 215, 311–318.

Wu, T., Brennan, M, 1998. Basic analytical study of pantograph-catenary system dynamics. Vehicle System Dynamics, 30, 443–456.